

Phonon properties of BaFe_2X_3 (X=S, Se) spin ladder compounds

Z. V. Popović, M. Šćepanović, N. Lazarević, and M. Opačić

*Center for Solid State Physics and New Materials, Institute of Physics Belgrade,
University of Belgrade, Pregrevica 118, 11080 Belgrade, Serbia*

M. M. Radonjić and D. Tanasković

*Scientific Computing Laboratory, Institute of Physics Belgrade,
University of Belgrade, Pregrevica 118, 11080 Belgrade, Serbia*

Hechang Lei[§] and C. Petrović

*Condensed Matter Physics and Materials Science Department,
Brookhaven National Laboratory, Upton, New York 11973-5000, USA*

(Dated: May 20, 2014)

We present the Raman scattering spectra of the S=2 spin ladder compounds BaFe_2X_3 (X=S, Se) in a temperature range between 20 K and 400 K. Although the crystal structures of these two compounds are both orthorhombic and very similar, they are not isostructural. The unit cell of BaFe_2S_3 (BaFe_2Se_3) is base-centered $Cmcm$ (primitive $Pnma$) giving totally 18 (36) modes to be observed in the Raman scattering experiment. We have detected almost all Raman active modes, predicted by factor group analysis, which can be observed from the cleavage planes of these compounds. Assignment of the observed Raman modes of $\text{BaFe}_2\text{S}(\text{Se})_3$ is supported by the lattice dynamics calculations. The antiferromagnetic long-range spin ordering in BaFe_2Se_3 below $T_N=255$ K leaves a fingerprint both in the A_{1g} and B_{3g} phonon mode linewidth and energy.

PACS numbers: 78.30.-j; 63.20.D-; 75.50.-y; 74.70.Xa

I. INTRODUCTION

The iron-based compounds are one of the top research fields in the condensed matter physics¹. These materials are not only superconducting² but also form low-dimensional magnetic structures – spin-chains, spin-ladders or spin-dimers,³ similar as in the case of cuprates⁴ or vanadates.⁵ Properties of iron-based selenide superconductors and other low dimensional magnetic phases of iron-chalcogenides are recently reviewed in Ref. 6.

BaFe_2S_3 and BaFe_2Se_3 belong to the family of the iron-based $S=2$ two-leg spin-ladder compounds. The crystal structure of these materials can be described as alternate stacking of Fe-S(Se) layers and Ba cations along the crystallographic a -axis (b -axis). In the Fe-S(Se) plane, only one-dimensional (1D) double chains of edge-shared $[\text{FeS}(\text{Se})]_4$ tetrahedra propagate along the a -axis (b -axis), as shown in Figure 1. Although the crystal structures of the BaFe_2S_3 and BaFe_2Se_3 are isomorphic, they are not isostructural. BaFe_2S_3 crystallizes in a base-centered orthorhombic structure with $Cmcm$ space group.⁷ The unit cell of BaFe_2Se_3 is also orthorhombic but primitive of the $Pmna$ space group. The main crystal structure difference of these compounds is an alternation of the Fe-Fe distances in BaFe_2Se_3 along the chain direction which does not exist in BaFe_2S_3 , where all distances between Fe atoms along the chain direction are the same, see Fig.1(b), and Fig.1(c). This difference probably leads to the diverse magnetic properties of these two compounds at low temperatures.

BaFe_2S_3 is quasi-one-dimensional semiconductor. The magnetic susceptibility of BaFe_2S_3 , measured at 100 Oe,

showed the divergence of the field-cooled susceptibility and zero-field-cooled susceptibility with the cusp at 25 K (freezing temperature)⁸ indicating the presence of short-range magnetic correlations and spin-glass-like behavior below 25 K. On the basis of these observations Gönen *et al.*⁸ proposed that each $[\text{Fe}_2\text{S}_3]^{2-}$ -chain possess strong intrachain antiferromagnetic coupling of Fe ions that is mediated through the sulfide ions. The combination of antiferromagnetic coupling, additional crystal field splitting due to neighboring Fe atoms, and direct Fe-Fe interactions presumably give rise to $S=0$ ground states in this compound.⁸

BaFe_2Se_3 is an insulator down to the lowest measured temperature with a long-range antiferromagnetic (AFM) order with T_N around 255 K and short-range AFM order at higher temperatures.^{9–12} It was shown that a dominant order involves 2×2 blocks of ferromagnetically aligned four iron spins, whereas these blocks order antiferromagnetically, in the same manner as the block-AFM $\sqrt{5}\times\sqrt{5}$ state of the iron-vacancy ordered $\text{A}_2\text{Fe}_4\text{Se}_5$.^{13–15}

To the best of our knowledge there are no data about the phonon properties of these compounds. In this paper we have measured polarized Raman scattering spectra of BaFe_2X_3 (X=S, Se) in the temperature range between 20 and 400 K. We have observed the Raman active optical phonons, which are assigned using polarized measurements and the lattice dynamical calculations. At temperatures below $T_N=255$ K in BaFe_2Se_3 the Raman modes shows an abrupt change of energy and linewidth due to the antiferromagnetic spin ordering.

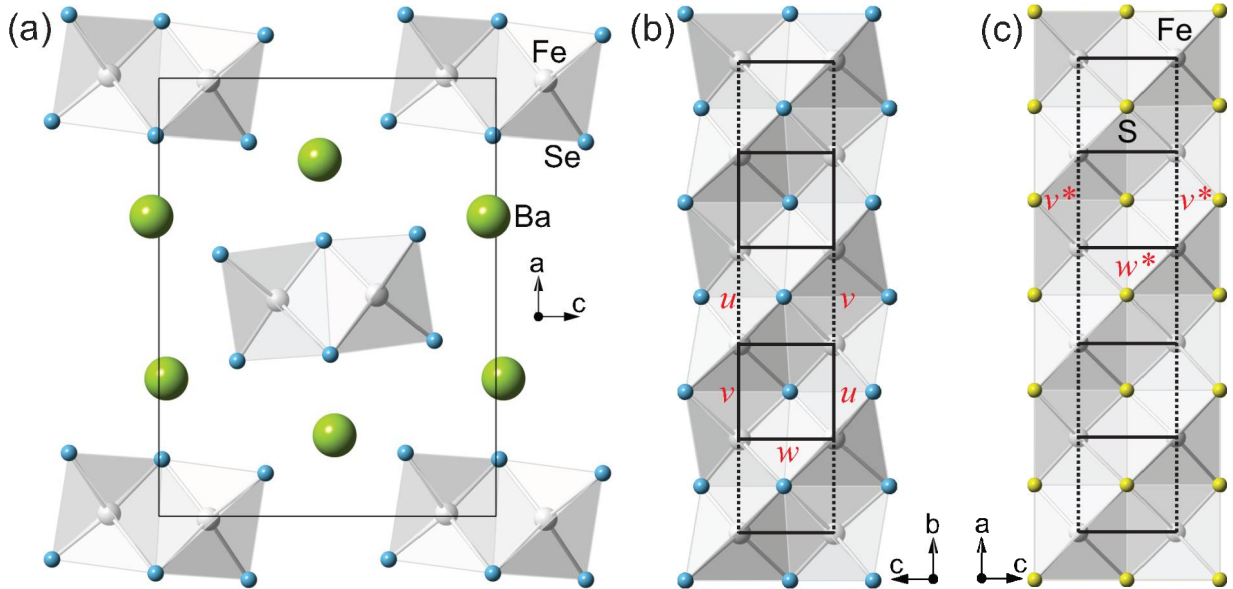


FIG. 1. (Color online) Schematic representation of the BaFe_2X_3 ($\text{X}=\text{S}, \text{Se}$) crystal structure. (a) Projection of the BaFe_2Se_3 crystal structure in the (ac) plane. (b) The double chain of Fe-Sc tetrahedra connected via common edges along the b -axis. (c) The Fe-S double chain in the (010) projection. w, u, v represents Fe-Fe distances of ladder rungs ($w=0.2697 \text{ nm}$; $w^*=0.2698 \text{ nm}$) and legs ($u=0.2688 \text{ nm}$, $v=0.2720 \text{ nm}$; $v^*=0.2643 \text{ nm}$). Note that in the case of BaFe_2S_3 the Fe atoms form an "ideal" ladder (all Fe-Fe distances along the ladder legs are equivalent, which is not a case in BaFe_2Se_3).

II. EXPERIMENT AND NUMERICAL METHOD

Single crystals of BaFe_2X_3 ($\text{X}=\text{S}, \text{Se}$) were grown using self-flux method with nominal composition $\text{Ba:Fe:X}=1:2:3$. Details were described in Ref. 16. Raman scattering measurements were performed on (110)(sulphide) [(100) (selenide)]-oriented samples in the backscattering micro-Raman configuration. Low temperature measurements were performed using KONTI CryoVac continuous flow cryostat coupled with JY T64000 and TriVista 557 Raman systems. The 514.5 nm line of an Ar^+/Kr^+ mixed gas laser was used as excitation source. The Raman scattering measurements at higher temperatures were done using LINKAM THMS600 heating stage.

We calculated phonon energies of the nonmagnetic $\text{BaFe}_2\text{S}(\text{Se})_3$ single crystals at the center of Brillouin zone. Calculations were performed within the theory of linear response using the density functional perturbation theory¹⁷ as implemented in QUANTUM ESPRESSO package.¹⁸ In the first step, we obtained the electronic structure by applying the pseudopotentials based on the projected augmented waves method with the Perdew-Burke-Ernzerhof exchange-correlation functional and nonlinear core correction. Used energy cutoffs for the wave functions and electron densities were 80 (64) Ry and 960 (782) Ry for $\text{BaFe}_2\text{S}(\text{Se})_3$, respectively. We have carried out the calculation with experimental values of the $\text{BaFe}_2\text{S}(\text{Se})_3$ unit cell parameters $a=0.87835 \text{ nm}$, $b=1.1219 \text{ nm}$, $c=0.5286 \text{ nm}$ ⁷ ($a=1.18834 \text{ nm}$, $b=0.54141 \text{ nm}$, $c=0.91409 \text{ nm}$ ¹¹), and the relaxed fractional coordi-

nates, see Table I. Relaxation was applied to place atoms in their equilibrium positions in respect to used pseudopotentials (all forces acting on every atom were smaller than 10^{-4} Ry/a.u.). The difference between experimental and relaxed coordinates is less than 3% for almost all atom coordinates, except for x direction of the Ba atoms in BaFe_2Se_3 , which is 6%. Reduction of the x coordinate of Ba atoms by relaxation leads to an increase of the distance between the Ba layers. The Brillouin zone was sampled with $8\times 8\times 8$ Monkhorst-Pack \mathbf{k} -space mesh. Calculated Γ point phonon energies of the BaFe_2S_3 and BaFe_2Se_3 are listed in Table II and Table IV, respectively.

TABLE I. Experimental and relaxed [in square brackets] fractional coordinates of BaFe_2S_3 (Ref. 7) and BaFe_2Se_3 (Ref. 11) crystal structures.

| Atom | Site | x | y | z |
|----------------------------|------|-----------------|-----------------|---------------|
| BaFe_2S_3 | | | | |
| Ba | (4c) | 0.50 [0.50] | 0.1859 [0.1817] | 0.25 [0.25] |
| Fe | (8e) | 0.3464 [0.3553] | 0.50 [0.50] | 0.00 [0.00] |
| S1 | (4c) | 0.50 [0.50] | 0.6147 [0.6051] | 0.25 [0.25] |
| S2 | (8g) | 0.2074 [0.2108] | 0.3768 [0.3945] | 0.25 [0.25] |
| BaFe_2Se_3 | | | | |
| Ba | (4c) | 0.186 [0.175] | 0.25 [0.25] | 0.518 [0.513] |
| Fe | (8d) | 0.493 [0.490] | 0.002 [-0.001] | 0.353 [0.358] |
| Se1 | (4c) | 0.355 [0.366] | 0.25 [0.25] | 0.233 [0.230] |
| Se2 | (4c) | 0.630 [0.613] | 0.25 [0.25] | 0.491 [0.485] |
| Se3 | (4c) | 0.402 [0.415] | 0.25 [0.25] | 0.818 [0.809] |

III. RESULTS AND DISCUSSION

A. BaFe₂S₃

The BaFe₂S₃ crystal symmetry is orthorhombic, space group *Cmcm* and $Z=4$.⁷ The site symmetries of atoms in *Cmcm* space group are C_{2v}^y (Ba, S1), C_2^x (Fe) and C_s^{xy} (S2). Factor group analysis yields:

$$(C_{2v}^y) : \Gamma = A_g + B_{1g} + B_{3g} + B_{1u} + B_{2u} + B_{3u},$$

$$(C_2^x) : \Gamma = A_g + 2B_{1g} + 2B_{2g} + B_{3g} + A_u + 2B_{1u} + 2B_{2u} + B_{3u}.$$

$$(C_s^{xy}) : \Gamma = 2A_g + 2B_{1g} + B_{2g} + B_{3g} + A_u + B_{1u} + 2B_{2u} + 2B_{3u}.$$

Summarizing these representations and subtracting the acoustic ($B_{1u}+B_{2u}+B_{3u}$) and silent ($2A_u$) modes, we obtained the following irreducible representations of BaFe₂S₃ vibrational modes:

$$\Gamma_{BaFe_2S_3}^{optical} = 5A_g(xx, yy, zz) + 6B_{1g}(xy) + 3B_{2g}(xz) + 4B_{3g}(yz) + 4B_{1u}(E \parallel z) + 5B_{2u}(E \parallel y) + 4B_{3u}(E \parallel x)$$

Thus 18 Raman and 13 infrared active modes are expected to be observed in the BaFe₂S₃ infrared and Raman spectra. Because our BaFe₂S₃ single crystal samples have (110)-orientation, we were able to observe all symmetry modes in the Raman scattering experiment.

The polarized Raman spectra of BaFe₂S₃, measured from (110)-plane at 100 K are given in Figure 2. Five A_g symmetry modes at about 39, 157, 165, 301 and 373 cm⁻¹ (100 K) are clearly observed for the $x'(zz)x'$ polarization configuration ($x'=[110]$, $y'=[\bar{1}\bar{1}0]$, $z=[001]$). For parallel polarization along the y' -axis the A_g and B_{1g} symmetry modes may be observed. By comparison ($y'y'$) with (zz) polarized spectrum we assigned the modes at 48, 133, 214, 332 and 381 cm⁻¹ as the B_{1g} ones. For the $x'(y'z)x'$ polarization configuration both the B_{2g} and the B_{3g} symmetry modes can be observed. Because we cannot distinguish the B_{2g} and B_{3g} by selection rules from the (110) plane the assignment of these modes (done with help of the lattice dynamics calculation, see Table II), should be taken as tentative.

The normal modes of some of A_g , B_{1g} and B_{3g} vibrations, obtained by the lattice dynamics calculations, are given as insets in Figures 2 and 3. According to these representations the lowest energy A_g^1 mode (39 cm⁻¹) originates from the Ba atom vibrations along the y -axis, the A_g^2 mode (157 cm⁻¹) represents dominantly S atom vibrations, which tend to elongate [Fe₂S₃]²⁻-chains along the y -axis. The A_g^3 mode originates from both the sulphur and the iron atoms vibrations, which tend to stretch ladders along the x -axis. The A_g^4 mode (Fig. 3) is sulphur atoms breathing vibrations, and the A_g^5 symmetry mode represents the S and Fe atom vibrations with opposite tendency. The Fe atoms vibrate in opposite directions along the x -axis elongating the ladder, together

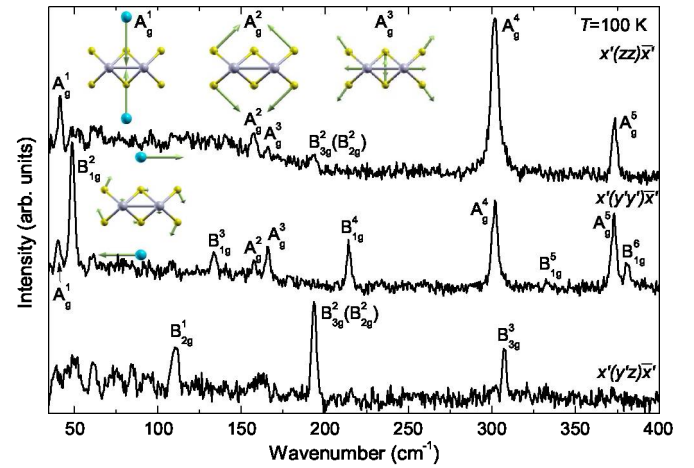


FIG. 2. (Color online) The polarized Raman scattering spectra of BaFe₂S₃ single crystal measured at 100 K. Insets are the normal modes of the A_g^1 , A_g^2 , A_g^3 , and B_{1g}^2 vibrations. $x'=[110]$, $y'=[\bar{1}\bar{1}0]$, $z=[001]$.

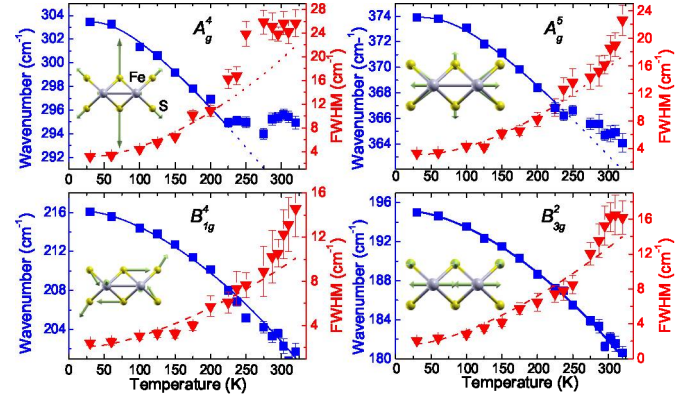


FIG. 3. (Color online) Experimental values (symbols) and anharmonic temperature dependence (solid and dashed lines) of BaFe₂S₃ Raman mode energies and broadenings. Insets represent the normal modes of the A_g^4 , A_g^5 , B_{1g}^4 , and B_{3g}^2 vibrations.

with S atom vibrations, which tend to compress ladder structure.

Temperature dependence of the A_g^4 , A_g^5 , B_{1g}^4 and B_{3g}^2 mode energy and linewidth are given in Figure 3. Solid and dashed lines are anharmonic temperature dependence of Raman mode energy and broadening, respectively. Influence of the anharmonic effects on the Raman mode energy and linewidth is taken into account via three (BaFe₂Se₃) and four (BaFe₂S₃)-phonon processes¹⁹ using relations:

$$\omega(T) = \omega_0 - C \left(1 + \frac{2}{e^{\hbar\omega_0/2k_B T} - 1} \right) + D \left(1 + \frac{3}{e^{\hbar\omega_0/3k_B T} - 1} + \frac{3}{(e^{\hbar\omega_0/3k_B T} - 1)^2} \right),$$

$$\Gamma(T) = \Gamma_0 + A \left(1 + \frac{2}{e^{\hbar\omega_0/2k_B T} - 1} \right) +$$

$$B \left(1 + \frac{3}{e^{\hbar\omega_0/3k_B T} - 1} + \frac{3}{(e^{\hbar\omega_0/3k_B T} - 1)^2} \right),$$

where ω_0 and Γ_0 are the temperature independent contribution to the Raman mode energy and the intrinsic linewidth, respectively. C, D, A , and B are the anharmonic constants. Anharmonic parameters, obtained as the best fit values are collected in Table III.

The most intriguing finding in Fig. 3 is a dramatic change of slope of the A_g^4 mode linewidth (energy) temperature dependence at about 275 K. Because a hump in the inverse molar magnetic susceptibility⁸, as well as a change of slope of the electrical resistivity²⁰ temperature dependence are observed in BaFe₂S₃ at about the same temperature we concluded that the deviation from anharmonic behaviour for A_g^4 mode could be spin- and charge-related. In fact, many of iron-based spin-ladder materials have the 3D-antiferromagnetic phase transition at about 260 K. We believe that in the case of BaFe₂S₃ the antiferromagnetic ordering of spins within the ladder legs changes from short-range to the long range state, without 3D antiferromagnetic spin ordering (the Néel state) of the whole crystal. This transition is followed with change of the electronic structure, which could explain the abrupt increase of the resistivity at this temperature²⁰. A lack of the BaFe₂S₃ low temperature crystallographic and transport properties measurements did not allow a more detailed study of a possible origin of the phonon energy and linewidth deviation from the anharmonic picture at about 275 K.

B. BaFe₂Se₃

The BaFe₂Se₃ unit cell consists of four formula units comprising of 24 atoms. The site symmetries of atoms in *Pnma* space group are C_s^{xz} (Ba, Se1, Se2, Se3) and C_1 (Fe). Factor group analysis yields:

$$(C_s^{xz}) : \Gamma = 2A_g + 1B_{1g} + 2B_{2g} + 1B_{3g} + A_u + 2B_{1u} + 1B_{2u} + 2B_{3u},$$

$$(C_1) : \Gamma = 3A_g + 3B_{1g} + 3B_{2g} + 3B_{3g} + 3B_{1u} + 3B_{2u} + 3B_{3u}.$$

Summarizing these representations and subtracting the acoustic ($B_{1u} + B_{2u} + B_{3u}$) and silent ($4A_u$) modes, we obtained the following irreducible representations of BaFe₂Se₃ vibrational modes:

$$\Gamma_{BaFe_2Se_3}^{optical} = 11A_g + 7B_{1g} + 11B_{2g} + 7B_{3g} + 11B_{1u} + 7B_{2u} + 11B_{3u}$$

Thus 36 Raman and 29 infrared active modes are expected to be observed in the BaFe₂Se₃ vibrational spectra. Because the BaFe₂Se₃ single crystals have the (100)-orientation (the crystallographic *a*-axis is perpendicular to the plane of the single crystal), we were able to access only the A_g and the B_{3g} symmetry modes in the Raman scattering experiment.

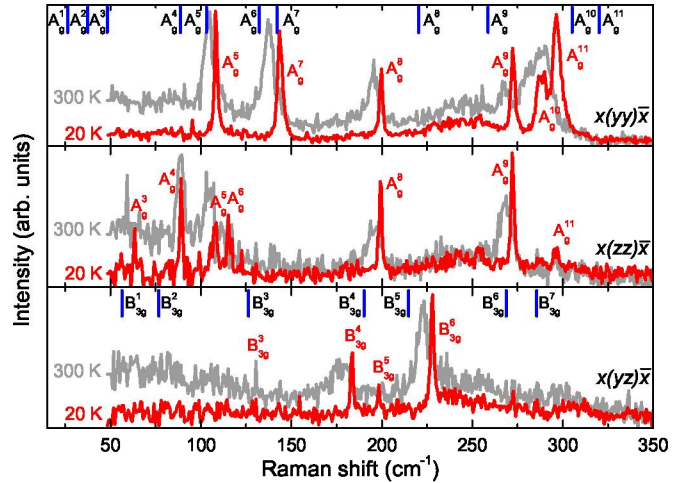


FIG. 4. (Color online) The $x(yy)\bar{x}$, $x(zz)\bar{x}$ and $x(yz)\bar{x}$ polarized Raman scattering spectra of BaFe₂Se₃ single crystals measured at room temperature and at 20 K. Vertical bars are calculated values of the A_g and the B_{3g} symmetry Raman active vibrations.

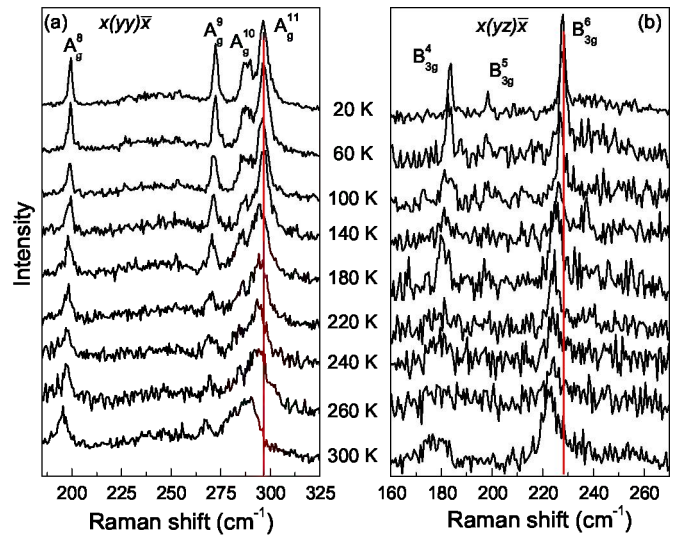


FIG. 5. The polarized Raman spectra of BaFe₂Se₃ single crystals measured at various temperatures. (a) $x(yy)\bar{x}$ polarization configuration; (b) $x(yz)\bar{x}$ polarization configuration.

The polarized Raman spectra of BaFe₂Se₃, measured from (100)-plane at room temperature and 20 K, for the parallel and crossed polarization configurations, are given in Figure 4. The spectra measured for parallel polarization configurations consist of the A_g symmetry modes. Six modes at about 108, 143.5, 200, 272, 288.7 and 296.5 cm⁻¹ (20 K) are clearly observed for the $x(yy)\bar{x}$ polarization configuration and three additional modes are observed at about 63.4, 89, and 115 cm⁻¹ for the $x(zz)\bar{x}$ polarization configuration. For the $x(yz)\bar{x}$ polarization configuration three Raman active B_{3g} symmetry modes at 183.8, 198 and 228 cm⁻¹ (20 K) are observed. Vertical bars in Fig. 4 denote the calculated energies of the A_g and B_{3g} symmetry modes, which are in rather good

TABLE II. Calculated and experimentally observed values of Raman active phonon mode energies (in cm^{-1}) of BaFe_2S_3 single crystal.

| Symmetry | Calculation relax.(unrelax.) | Experiment | | Activity | Symmetry | Calculation | Experiment | | Activity |
|------------|---------------------------------|------------|-------|--------------|------------|---------------|------------|-------|----------|
| | | 300 K | 100 K | | | | 300 K | 100 K | |
| A_g^1 | 42.3 (51.2) | | 39 | (xx, yy, zz) | B_{1g}^1 | 16.7 (63) | | | (xy) |
| A_g^2 | 154.2 (156) | | 157 | " | B_{1g}^2 | 55.1 (81.8) | 44 | 48 | " |
| A_g^3 | 201.9 (167.4) | 152 | 165 | " | B_{1g}^3 | 138.8 (153.1) | 127 | 133 | " |
| A_g^4 | 366.9 (294.8) | 295 | 301 | " | B_{1g}^4 | 243.5 (221.9) | 203 | 214 | " |
| A_g^5 | 385.8 (307.1) | 365 | 372 | " | B_{1g}^5 | 337.8 (241.6) | | 332 | " |
| | | | | | B_{1g}^6 | 400.2 (330) | 374 | 381 | " |
| B_{2g}^1 | 107.8 (113.7) | 107 | 109 | (xz) | B_{3g}^1 | 55.1 (66.8) | | | (yz) |
| B_{2g}^2 | 224.1 (180.8) | 181 | 193 | " | B_{3g}^2 | 201.1 (171.1) | 181 | 193 | " |
| B_{2g}^3 | 347.8 (283.6) | | | " | B_{3g}^3 | 311.2 (308.7) | 297 | 307 | " |
| | | | | | B_{3g}^4 | 369.3 (351.7) | | | " |

TABLE III. Anharmonic fit parameters (in cm^{-1}) of BaFe_2S_3 and BaFe_2Se_3 .

| Mode symmetry | ω_0 | Γ_0 | C | D | A | B |
|----------------------------|------------|------------|------|-----|-----|-----|
| BaFe_2S_3 | | | | | | |
| A_g^4 | 309.7 | 0 | 5.9 | 0.3 | 2 | 1.1 |
| A_g^5 | 381.0 | 0 | 6.9 | 0.2 | 1.8 | 1.3 |
| B_{1g}^4 | 217.8 | 0.9 | 1.2 | 0.4 | 1.0 | 0.2 |
| B_{3g}^2 | 196.4 | 0 | 1.0 | 0.3 | 1.4 | 0.2 |
| BaFe_2Se_3 | | | | | | |
| A_g^8 | 201.3 | | 1.48 | | | |
| A_g^9 | 275.2 | | 2.75 | | | |
| A_g^{10} | 292.7 | | 4.3 | | | |
| A_g^{11} | 301.0 | | 4.1 | | | |

agreement with experimentally observed ones. The results of the lattice dynamics calculations, together with the experimental data are summarized in Table IV.

According to the lattice dynamics calculations the lowest energy A_g^1 mode is dominated by Ba atom vibrations along the $\langle 101 \rangle$ directions, the A_g^2 mode represents vibrations of Fe and Se atoms which tend to rotate $[\text{Fe}_2\text{Se}_3]^{2-}$ -chains around of the b -axis. The A_g^3 mode involves all atoms vibrations, which tend to stretch crystal structure along the $\langle 101 \rangle$ directions, whereas the A_g^4 mode originates from Se atom vibrations along the c -axis and the Fe atom vibrations along the $\langle 101 \rangle$ directions. The A_g^5 mode represents vibration of Fe and Se atoms, which lead to $[\text{Fe}_2\text{Se}_3]^{2-}$ -chain compression along the c -axis. The A_g^6 mode originates from Se and Fe atom vibrations which stretch $[\text{Fe}_2\text{Se}_3]^{2-}$ -chains along the c -axis. Finally, the A_g^7 mode originates from Fe atom vibrations toward each other along the chain direction together with vibrations of the Se atoms along the c -axis. The normal coordinates of the A_g^8 , A_g^9 , A_g^{10} , and A_g^{11} modes are given as insets in Figure 6. As can be seen from Fig. 6 the A_g^8 mode originates dominantly from Se atom stretching vi-

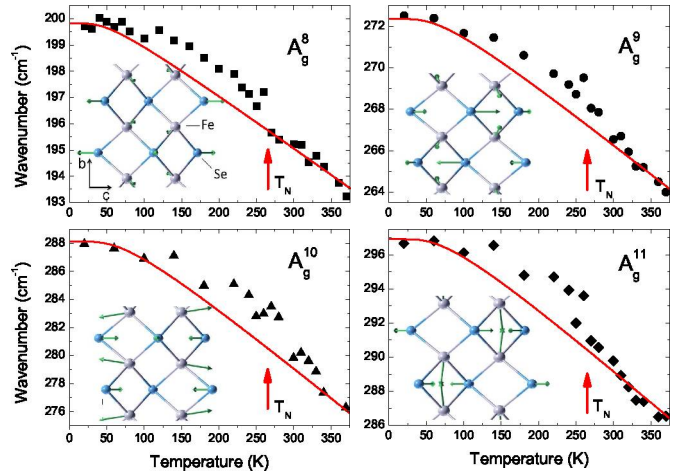


FIG. 6. (Color online) Experimental values (symbols) and anharmonic temperature dependence (solid lines) of BaFe_2Se_3 Raman mode energies. Influence of the anharmonic effects on the Raman mode energy is taken into account via three-phonon processes¹⁹, see text. Anharmonic parameters, obtained as the best fit values for the temperature range above T_N , are given in Table III. Insets represent normal modes of the A_g^8 , A_g^9 , A_g^{10} , and A_g^{11} vibrations.

brations, whereas the A_g^9 , A_g^{10} , and A_g^{11} modes represent vibrations of both the Se and Fe atoms. In fact, the A_g^9 mode represents mostly Se atom vibrations along the c -axis, the A_g^{10} mode consists of Fe and Se vibrations along the c -axis, which tend to elongate ladder structure along the b -axis. Finally, the A_g^{11} mode represents the Fe atom vibrations toward each other along the chain axis together with Se atom vibrations perpendicular to the chain direction.

By lowering the temperature the lattice parameters of BaFe_2Se_3 decrease continuously without the crystal symmetry change around the magnetic ordering temperature^{11,12} $T_N=255$ K. Consequently we should expect the Raman mode hardening, following the anhar-

TABLE IV. Calculated and experimentally observed values of Raman active phonon mode energies (in cm^{-1}) of BaFe_2Se_3 single crystal.

| Symmetry | Calc. | Experiment | | Activity | Symmetry | Calc. | Experiment | | Activity |
|------------|-------|------------|-------|--------------|---------------|-------|------------|-------|----------|
| | | 300 K | 20 K | | | | 300 K | 20 K | |
| A_g^1 | 26.5 | | | (xx, yy, zz) | B_{2g}^1 | 25.8 | | | (xz) |
| A_g^2 | 37.5 | | | " | B_{2g}^2 | 48.0 | | | " |
| A_g^3 | 48.3 | 59 | 63.4 | " | B_{2g}^3 | 68.7 | | | " |
| A_g^4 | 88.6 | 88 | 89 | " | B_{2g}^4 | 88.8 | | | " |
| A_g^5 | 103.0 | 104.3 | 108 | " | B_{2g}^5 | 100.4 | | | " |
| A_g^6 | 132.4 | 111 | 115 | " | B_{2g}^6 | 138.2 | | | " |
| A_g^7 | 142.0 | 137 | 143 | " | B_{2g}^7 | 144.5 | | | " |
| A_g^8 | 220.4 | 195.6 | 200 | " | B_{2g}^8 | 212.9 | | | " |
| A_g^9 | 258.8 | 267 | 272 | " | B_{2g}^9 | 261.7 | | | " |
| A_g^{10} | 305.2 | 280 | 288.7 | " | B_{2g}^{10} | 303.9 | | | " |
| A_g^{11} | 320.2 | 290 | 296.5 | " | B_{2g}^{11} | 321.5 | | | " |
| B_{1g}^1 | 56.4 | | | (xy) | B_{3g}^1 | 56.4 | | | (yz) |
| B_{1g}^2 | 72.8 | | | " | B_{3g}^2 | 76.7 | | | " |
| B_{1g}^3 | 126.2 | | | " | B_{3g}^3 | 126.4 | | | " |
| B_{1g}^4 | 191.4 | | | " | B_{3g}^4 | 190.2 | 177 | 183.8 | " |
| B_{1g}^5 | 210.5 | | | " | B_{3g}^5 | 214.9 | | 198 | " |
| B_{1g}^6 | 267.1 | | | " | B_{3g}^6 | 268.8 | 222.8 | 228 | " |
| B_{1g}^7 | 285.2 | | | " | B_{3g}^7 | 285.7 | | | " |

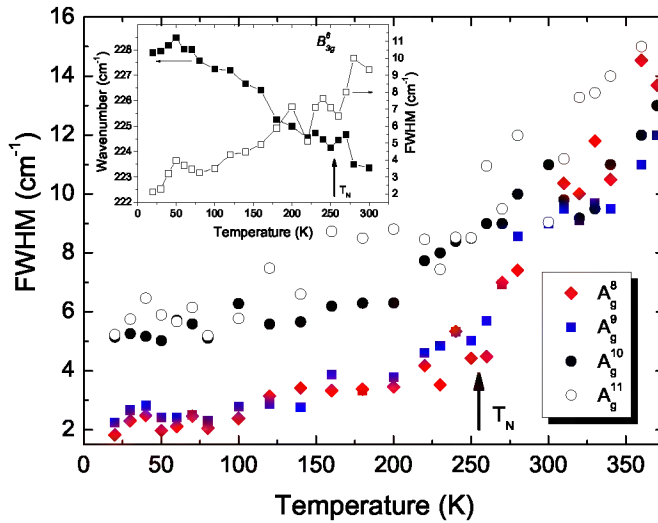


FIG. 7. Linewidth vs temperature dependence of the A_g^8 , A_g^9 , A_g^{10} , and A_g^{11} modes. Inset: Energy and linewidth temperature dependence of the B_{3g}^6 mode

monic phonon mode temperature dependance¹⁹ without any abrupt change. Contrary to the expectations the A_g and B_{3g} modes (see Figure 5) increase their energies and sharply reduce the linewidth below the phase transition temperature T_N , as it is shown in details in the Figures 6 and 7. Because a significant local lattice distortion (Fe atom displacement along the b -axis is as large as approximately 0.001 nm)^{11,12} exists, driven by the mag-

netic order, we concluded that spin-phonon (magnetoelectric) coupling is responsible for Raman mode energy and linewidth change in the antiferromagnetic phase. In fact, the existence of local displacements in the Fe atoms at T_N have a significant impact on the electronic structure due to rearrangement of electrons near the Fermi level¹¹ and consequently the change in the phonon energy and broadening. Raman mode energy change at about T_N is clearly observed as deviation from the usual anharmonicity temperature dependence (solid lines in Figs. 6 and 7) for all modes presented in Figs. 6 and 7.

IV. CONCLUSION

We have measured the polarized Raman scattering spectra of the BaFe_2S_3 and BaFe_2Se_3 single crystals in a temperature range between 20 K and 400 K. Almost all Raman-active modes predicted by factor-group analysis to be observed from the cleavage planes of BaFe_2S_3 (110) and BaFe_2Se_3 (100) single crystals, are experimentally detected and assigned. Energies of these modes are in rather good agreement with the lattice dynamics calculations. The BaFe_2Se_3 Raman modes linewidth and energy, change substantially at temperatures below $T_N=255$ K, where this compound becomes antiferromagnetically long-range ordered.

V. ACKNOWLEDGMENTS

This work was supported by the Serbian Ministry of Education, Science and Technological Development under Projects ON171032, ON171017 and III45018. Work at Brookhaven was supported by the Center for Emergent Superconductivity, an Energy Frontier Research Center

funded by the US DOE, Office for Basic Energy Science (H.L. and C.P.). Numerical simulations were run on the AEGIS e-Infrastructure, supported in part by FP7 projects EGI-InSPIRE and PRACE-3IP.

[§]Present address: Frontier Research Center, Tokyo Institute of Technology, 4259 Nagatsuta, Midori, Yokohama 226-8503, Japan.

-
- ¹ C. King and D. A. Pendlebury, Web of knowledge research fronts 2013, 100 Top-Ranked Specialties in the Sciences and Social Sciences, <http://sciencewatch.com/sites/sw/files/sw-article/media/research-fronts-2013.pdf>.
- ² Y. Kamihara, T. Watanabe, M. Hirano, and H. Hosono, *J. Am. Chem. Soc.* **130**, 3296 (2008).
- ³ Z. V. Popović, M. Šeepanović, N. Lazarević, M. M. Radonjić, D. Tanasković, H. Lei, and C. Petrović, *Phys. Rev. B* **89**, 014301 (2014).
- ⁴ Z. V. Popović, M. J. Konstantinović, V. A. Ivanov, O. P. Khuong, R. Gajić, A. Vietkin, and V. V. Moshchalkov, *Phys. Rev. B* **62**, 4963 (2000).
- ⁵ M. J. Konstantinović, Z. V. Popović, M. Isobe, and Y. Ueda, *Phys. Rev. B* **61**, 15185 (2000).
- ⁶ E. Dagotto, *Rev. Mod. Phys.* **85**, 849 (2013).
- ⁷ H. Hong and H. Steinfink, *Journal of Solid State Chemistry* **5**, 93 (1972).
- ⁸ Z. S. Gönen, P. Fournier, V. Smolyaninova, R. Greene, F. M. Araujo-Moreira, and B. Eichhorn, *Chemistry of Materials* **12**, 3331 (2000).
- ⁹ H. Lei, H. Ryu, A. I. Frenkel, and C. Petrović, *Phys. Rev. B* **84**, 214511 (2011).
- ¹⁰ B. Saparov, S. Calder, B. Sipos, H. Cao, S. Chi, D. J. Singh, A. D. Christianson, M. D. Lumsden, and A. S. Sefat, *Phys. Rev. B* **84**, 245132 (2011).
- ¹¹ J. M. Caron, J. R. Neilson, D. C. Miller, A. Llobet, and T. M. McQueen, *Phys. Rev. B* **84**, 180409 (2011).
- ¹² Y. Nambu, K. Ohgushi, S. Suzuki, F. Du, M. Avdeev, Y. Uwatoko, K. Munakata, H. Fukazawa, S. Chi, Y. Ueda, and T. J. Sato, *Phys. Rev. B* **85**, 064413 (2012).
- ¹³ F. Ye, S. Chi, W. Bao, X. F. Wang, J. J. Ying, X. H. Chen, H. D. Wang, C. H. Dong, and M. Fang, *Phys. Rev. Lett.* **107**, 137003 (2011).
- ¹⁴ N. Lazarević, M. Abeykoon, P. W. Stephens, H. Lei, E. S. Bozin, C. Petrović, and Z. V. Popović, *Phys. Rev. B* **86**, 054503 (2012).
- ¹⁵ N. Lazarević, H. Lei, C. Petrović, and Z. V. Popović, *Phys. Rev. B* **84**, 214305 (2011).
- ¹⁶ H. Lei, H. Ryu, V. Ivanovski, J. B. Warren, A. I. Frenkel, B. Cekic, W.-G. Yin, and C. Petrović, *Phys. Rev. B* **86**, 195133 (2012).
- ¹⁷ S. Baroni, S. de Gironcoli, A. Dal Corso, and P. Giannozzi, *Rev. Mod. Phys.* **73**, 515 (2001).
- ¹⁸ P. Giannozzi, S. Baroni, N. Bonini, M. Calandra, R. Car, C. Cavazzoni, D. Ceresoli, G. L. Chiarotti, M. Cococcioni, I. Dabo, A. D. Corso, S. de Gironcoli, S. Fabris, G. Fratesi, R. Gebauer, U. Gerstmann, C. Goucoussis, A. Kokalj, M. Lazzeri, L. Martin-Samos, N. Marzari, F. Mauri, R. Mazzarello, S. Paolini, A. Pasquarello, L. Paulatto, C. Sbraccia, S. Scandolo, G. Sclauzero, A. P. Seitsonen, A. Smogunov, P. Umari, and R. M. Wentzcovitch, *Journal of Physics: Condensed Matter* **21**, 395502 (2009).
- ¹⁹ M. Balkanski, R. F. Wallis, and E. Haro, *Phys. Rev. B* **28**, 1928 (1983).
- ²⁰ W. Reiff, I. Grey, A. Fan, Z. Eliezer, and H. Steinfink, *Journal of Solid State Chemistry* **13**, 32 (1975).